Archives of Hydro-Engineering and Environmental Mechanics
Vol. 56 (2009), No. 1–2, pp. 43–61

A Lagrangian Finite Element Analysis of Gravity Waves in Water of Variable Depth

Ryszard Staroszczyk

Institute of Hydro-Engineering PAS, ul. Kościerska 7, 80-328 Gdańsk-Oliwa, Poland,
e-mail: rstar@ibwpan.gda.pl

(Received December 19, 2008; revised May 15, 2009)

Abstract

The paper is concerned with the problem of gravitational wave propagation in water of variable depth. The problem is formulated in the Lagrangian description, and the ensuing equations are solved numerically by a finite element method. In computations a convecting mesh that follows the material fluid particles is used. As illustrations, results of numerical simulations carried out for plane gravity waves propagating over bottoms of simple geometry are presented. For parameters typical of a laboratory flume, the transformation of a transient wave, generated by a single movement of a piston-like wave maker, is investigated. The results show the evolution of the free-surface elevation, displaying steepening of the wave over sloping beds and its gradual attenuation in regions of uniform depth.

Key words: Gravity water wave, variable water depth, transient problem, Lagrangian formulation, finite element method.

Notation

$\boldsymbol{b}$ – body force vector,
c – speed of sound,
$\boldsymbol{D}$ – strain-rate tensor,
D_0 – wave-maker horizontal displacement amplitude,
$\boldsymbol{F}$ – referential deformation gradient tensor,
g – gravity acceleration,
$\boldsymbol{G}$ – spatial deformation gradient tensor,
H – still water depth,
$\boldsymbol{I}$ – unit tensor,
J – deformation Jacobian,
K – water compressibility modulus,
$\boldsymbol{n}$ – unit normal vector in spatial coordinates,
p – hydrostatic pressure,
$\boldsymbol{s}$ – unit tangential vector in spatial coordinates,

t – time,
$\boldsymbol{v}$ – velocity vector,
$\boldsymbol{x}, \boldsymbol{X}$ – spatial and referential position vectors,
∇^2 – Laplace operator,
μ – water viscosity,
ϱ, ϱ_0 – current and referential fluid densities,
$\boldsymbol{\sigma}$ – Cauchy stress tensor.

1. Introduction

The problem of propagation of free-surface gravitational waves in shallow water of variable depth is the one which has been extensively analysed by employing the methods of classical fluid mechanics. Examples of successful treatments can be found in fundamental treatises by Stoker (1957) and Wehausen and Laitone (1960), and more recently in two volumes of the book by Dingemans (1997).

The application of classical analytical solutions, though, especially of those based on a small parameter expansions, is usually restricted to the cases of small-amplitude waves, and to the water domains with beds of small slopes. In more challenging situations, that is for large-amplitude waves or/and the beds of significantly varying geometry, one has to resort to discrete methods. In these methods, approximate solutions of fluid flow problems are conventionally constructed by adopting the Eulerian (spatial) formulation of the flow governing equations. Such an approach has been proved successful in solving a wide variety of fluid mechanics problems, especially those involving domains with fixed boundaries. However, the numerical methods based on the Euler description fail in the cases in which the geometry of the flow domain changes rapidly in time. For instance, in fluid flows with free surfaces, or when the solid-liquid interaction, with a changing shape of the interface, takes place. The failure of the Eulerian-type methods is largely due to numerical difficulties associated with the sufficiently accurate tracing of moving boundaries enclosing a fluid domain. For this reason, over the past two decades, the methods based on the Lagrangian (material) description have gained in popularity, since the formulation of boundary conditions, which are specified on material surfaces (that is, on the surfaces which do not move in the Lagrangian coordinates) is straightforward. Further, the convective terms which enter the momentum equations cast in the spatial coordinates, do not appear in the material description, and therefore increased stability of numerical schemes can be achieved. The price of these computational gains, however, is the appearance in the governing equations of terms involving deformation gradient components and Jacobians. Several examples of the implementation of the Lagrangian formulation, using the finite element method, can be found in the papers by Ramaswamy and Kawahara (1987), Radovitzky and Ortiz (1998) and Parrinello and Borino (2007).

A characteristic feature of the conventional numerical Lagrangian method, in which fixed in space discrete meshes are used, is the problem with a proper treatment of large deformations, since the latter cause progressive accumulation of numerical errors as the material particles considerably depart from their initial positions (that is, the deformation gradient components reach large magnitudes). In order to reduce the above errors, a number of variants of the Lagrangian method have been devised in the recent years. These improved methods include, among others: the Arbitrary Lagrangian-Eulerian (ALE) method, used by Braess and Wriggers (2000), Souli and Zolesio (2001) and Rabier and Medale (2003), the Finite Point Method (FPM) employed by Oñate et al (1996), Löhner et al (2002) and Ortega et al (2007), and the Particle Finite Element Method (PFEM) applied by Idelsohn et al (2004), Aubry et al (2005) and Idelsohn et al (2006). Some aspects of the Lagrangian-type approaches are discussed in the book by Zienkiewicz and Taylor (2000a).

In this work, the Lagrangian formulation is employed to analyse the problem of non-linear surface gravity waves propagating in water of variable depth. The water is assumed to be a Newtonian viscous, compressible, and barotropic liquid. In the finite element implementation, an evolving mesh is used, the nodes of which are attached to a set of selected material fluid particles. Accordingly, the mesh is updated after each discrete time step, by convecting the mesh nodes as the corresponding fluid particles change their spatial positions during the flow. In this way, the material coordinates are changed every time step, so that the referential configuration at the start of a new time step coincides with the deformed configuration at the end of a preceding time step. By doing so, the numerical errors associated with the evaluation of the deformation gradient components are minimized, since the magnitudes of these components are always close to those of a unit tensor. The proposed numerical model has been used to simulate the plane problems of water wave propagation for several cases of simple bed profiles, idealizing the conditions encountered in natural surf zones. The simulations have been carried out for parameters pertaining to a laboratory wave flume, with the bottom consisting of segments of horizontal and uniformly sloping planes. Assuming that water is set in motion by a piston-type wave-maker, the behaviour of a transient surface wave generated by a single translational movement of the maker vertical wall is investigated. Hence, the transformation of the wave, including its steepening over inclined bottoms and progressive attenuation due to dispersion in regions of uniform depth, is examined. The results of numerical simulations illustrate the evolution of the water free surface, depending on a particular bed geometry and the slopes of the inclined parts of the bottom.

This paper is a sequel to an earlier work by the author (Staroszczyk 2007), in which a general Lagrangian framework for the treatment of Newtonian compressible fluids with two viscosity parameters was formulated, and which contains the details concerning the construction a finite element scheme, used later for the numerical

analysis of surface waves propagating over horizontal beds. Now the model is modified, by first formulating it in dimensionless variables, and then by extending it so that it can be applied to fluid flows over uneven beds. Also, some new features of a numerical nature have been added to the model to improve its robustness and computational performance.

The paper is structured as follows. In Section 2 the water flow governing equations are first formulated in the Eulerian coordinates, then re-scaled into dimensionless expressions, and finally transformed into the Lagrangian forms. The ensuing Navier-Stokes and continuity equations are solved by the finite element method, the main features of which are outlined in Section 3. The following Section 4 contains the results of the model applications to the wave propagation problems, involving three specific cases of the bottom profiles. Finally, some concluding remarks are given in Section 5.

2. Governing Equations

A plane wave propagation problem, depicted in Fig. 1, is considered, in which free-surface gravity waves propagate over an uneven bottom. The problem is analysed in Cartesian coordinates. Two coordinate frames are adopted: the spatial (Eulerian) frame Ox_1x_2 describing the motion of the fluid in the current (deformed) configuration, and the referential (Lagrangian) frame OX_1X_2 defining the positions of material particles at the reference time. The axes x_1 and X_1 are directed horizontally, and the vertical axes x_2 and X_2 are directed upwards. The bottom is treated as rigid and impermeable, and its, fixed in time, geometry is defined by the function $x_2 = f(x_1)$. The current position of the free water surface is described by the function $x_2 = h(x_1, t)$.

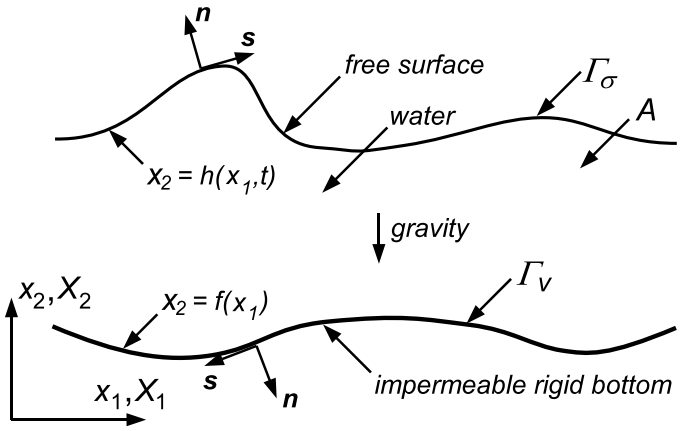

Fig. 1. Plane free-surface water wave propagation problem definition

Denote the current fluid particle velocity by the vector $\boldsymbol{v}$, with components $v_j(x_i, t)$, $(i, j = 1, 2)$. Then the mass conservation law, expressed in the spatial coordinates Ox_i, is given by the continuity equation

$$\frac{\mathrm{D}\varrho}{\mathrm{D}t} + \varrho \ \mathrm{div}\ \boldsymbol{v} = 0, \tag{1}$$

in which ϱ is the fluid density, $\mathrm{D}/\mathrm{D}t$ denotes the material time derivative, and div denotes the spatial divergence operator. The linear momentum conservation balance, in the presence of body forces, yields the equation of motion in the form

$$\varrho \frac{\mathrm{D}\boldsymbol{v}}{\mathrm{D}t} = \ \mathrm{div}\ \boldsymbol{\sigma} + \varrho \boldsymbol{b}, \tag{2}$$

where $\boldsymbol{\sigma}$ is the Cauchy stress tensor and $\boldsymbol{b}$ denotes the body force vector. In the problem investigated, the only body force is that due to gravity; hence, the vector $\boldsymbol{b}$ has the components $b_1 = 0$ and $b_2 = -g$, with g being the gravity acceleration.

Water is assumed here to be an isotropic, viscous and compressible fluid, the behaviour of which is defined by the following constitutive relation (Chadwick 1999):

$$\boldsymbol{\sigma} = -\left(p + \frac{2}{3}\mu \ \mathrm{tr}\ \boldsymbol{D}\right)\boldsymbol{I} + 2\mu \boldsymbol{D}. \tag{3}$$

In the above expression, p is the hydrostatic pressure, $\boldsymbol{D}$ is the strain-rate tensor, μ denotes the fluid viscosity, $\boldsymbol{I}$ is the unit tensor, and tr denotes the trace of a tensor. Substitution of the stress relation (3) into the motion equation (2) results in the Navier-Stokes equation expressed by

$$\varrho \frac{\mathrm{D}\boldsymbol{v}}{\mathrm{D}t} = -\mathrm{grad}\ p + \mu \nabla^2 \boldsymbol{v} + \frac{1}{3}\mu \ \mathrm{grad}\ \mathrm{div}\ \boldsymbol{v} + \varrho \boldsymbol{b}, \tag{4}$$

where grad denotes the spatial gradient operator, and $\nabla^2(\cdot) = \mathrm{div}\,[\mathrm{grad}(\cdot)^T]$ stands for the vector Laplacian operator in the spacial description.

A common approximation is to treat water as a barotropic fluid, for which the pressure is entirely determined by the fluid density. Adopting the pressure dependence on the density to be expressed by

$$\frac{\mathrm{D}\varrho}{\mathrm{D}t} = \frac{1}{c^2}\frac{\mathrm{D}p}{\mathrm{D}t}, \tag{5}$$

in which c is the speed of sound, and inserting the latter expression into Eq. (1), transforms the continuity equation into the form

$$\frac{\mathrm{D}p}{\mathrm{D}t} + K \ \mathrm{div}\ \boldsymbol{v} = 0, \tag{6}$$

where $K = \varrho c^2$ is the fluid elastic compressibility modulus.

Boundary conditions, which must be satisfied by the solutions of differential equations (5) and (6), are adopted in the standard forms. The free water surface at $x_2 = h(x_1, t)$ is supposed to be traction-free, which follows from the tacit assumption that the stresses within the fluid are measured relative to the atmospheric pressure, treated here as constant. Thus, at the upper boundary Γ_σ (see Fig. 1), the following conditions are imposed:

$$x_2 = h(x_1, t): \quad \boldsymbol{n} \cdot (\boldsymbol{\sigma}\boldsymbol{n}) = 0 \quad \text{and} \quad \boldsymbol{s} \cdot (\boldsymbol{\sigma}\boldsymbol{n}) = 0, \tag{7}$$

where $\boldsymbol{n}$ and $\boldsymbol{s}$ denote, respectively, the unit vectors normal and tangential to the Γ_σ boundary. At the rigid bottom, at $x_2 = f(x_1)$, the fluid velocity component normal to the boundary Γ_v is zero, and free-slip conditions are assumed at the bottom. The latter assumption implies that the effects of the boundary layer along the rigid bed are not accounted for, but it is supposed here that such viscous flow effects are negligibly small in the case of water waves propagating in a flume. Accordingly, the kinematic boundary condition at the bottom is expressed by

$$x_2 = f(x_1): \quad \boldsymbol{v} \cdot \boldsymbol{n} = 0, \tag{8}$$

that is, the tangential velocity components is unconstrained. Additional kinematic conditions must be specified for moving parts of the solid boundaries, for instance for a wave-maker wall, etc.

Equations (4) and (6) formulate the flow problem in the current configuration, that is, in the spatial coordinates Ox_1x_2. In order to describe the problem in the referential (material) coordinates OX_1X_2, the deformation gradient tensors are introduced into the analysis. Hence, the referential gradient, $\boldsymbol{F}$, and its spatial counterpart, $\boldsymbol{G}$, defined by

$$\boldsymbol{F}(\boldsymbol{X}, t) = \text{ Grad } \boldsymbol{x}(\boldsymbol{X}, t), \quad \boldsymbol{G}(\boldsymbol{x}, t) = \boldsymbol{F}^{-1}(\boldsymbol{x}, t) = \text{ grad } \boldsymbol{X}(\boldsymbol{x}, t), \tag{9}$$

are used. In the above expressions, $\boldsymbol{x}$ and $\boldsymbol{X}$ denote the fluid particle position vectors in the deformed and the referential coordinates, respectively, and Grad denotes the referential gradient operator. By applying some general relations that connect the differential operators grad and div in the current, and Grad and Div in the referential coordinates (Chadwick 1999), one can transform equations (4) and (6) into equivalent referential forms, see Staroszczyk (2007). The resulting Navier-Stokes equation, expressed in components, has the form

$$J^{-1}\varrho_0 \frac{\partial v_i}{\partial t} = -G_{ji}\frac{\partial p}{\partial X_j} + \mu\, G_{jm}G_{km}\frac{\partial^2 v_i}{\partial X_j}X_k + \frac{1}{3}\mu\, G_{jm}G_{ki}\frac{\partial^2 v_m}{\partial X_j}X_k + J^{-1}\varrho_0 b_i\,, \tag{10}$$

where the summation convention for repeated subscripts $(i, j, k, m = 1, 2)$ applies, and the continuity equation becomes

$$JK^{-1}\,\frac{\partial p}{\partial t} + G_{jk}\frac{\partial v_k}{\partial X_j} = 0. \tag{11}$$

In the latter two relations,

$$G_{ij} = \frac{\partial X_i}{\partial x_j} \quad (i, j = 1, 2), \quad J = \det \boldsymbol{F} = (\det \boldsymbol{G})^{-1} = \frac{\varrho_0}{\varrho}, \tag{12}$$

where J denotes the Jacobian of the deformation, and ϱ_0 is the fluid density in the referential configuration. Similarly, the boundary conditions, defined by Eq. (7) and (8), need to be expressed in the material coordinates. This is achieved by relating, via the deformation gradient components G_{ij}, the components of the unit vectors $\boldsymbol{n}$ and $\boldsymbol{s}$ in the Ox_1x_2 frame to their counterparts in the OX_1X_2 frame — for details see Staroszczyk (2007).

The above governing equations, (10) and (11), before solving them by a numerical method, are transformed into dimensionless forms so that the magnitudes of all unknown variables are of order unity. Accordingly, characteristic scales for the quantities involved in the flow description are introduced. From among many possible alternatives, the following scalings are employed in this analysis:

$$\begin{aligned} \left(\bar{x}_i, \bar{X}_i\right) &= \frac{(x_i, X_i)}{H^*}, \quad \bar{v}_i = \frac{v_i}{v^*}, \quad \bar{t} = \frac{t}{t^*}, \\ (\bar{\boldsymbol{\sigma}}, \bar{p}) &= \frac{(\boldsymbol{\sigma}, p)}{p^*}, \quad \bar{\boldsymbol{D}} = \frac{\boldsymbol{D}}{D^*}, \quad \bar{\mu} = \frac{\mu}{\mu^*}, \end{aligned} \tag{13}$$

where an over-bar indicates a dimensionless variable, and an asterisk denotes a scaling magnitude. Hence, H^* is a typical depth of water, and is used as a length unit, $v^* = \sqrt{gH^*}$ is a velocity unit, $t^* = H^*/v^*$ is a time unit, $p^* = \varrho_0 g H^* = \varrho_0 (v^*)^2$ is a stress unit, $D^* = v^*/H^*$ is a strain-rate unit, and $\mu^* = \varrho_0 v^* H^*$ is a viscosity unit.

By using the relations (13) to re-scale the spatial and temporal derivatives in Eq. (10) and (11), one arrives at the following non-dimensional forms of the Navier-Stokes and the continuity equations:

$$J^{-1} \frac{\partial \bar{v}_i}{\partial \bar{t}} = -G_{ji} \frac{\partial \bar{p}}{\partial \bar{X}_j} + \bar{\mu}\, G_{jm} G_{km} \frac{\partial^2 \bar{v}_i}{\partial \bar{X}_j\, \partial \bar{X}_k} + \frac{1}{3} \bar{\mu}\, G_{jm} G_{ki} \frac{\partial^2 \bar{v}_m}{\partial \bar{X}_j\, \partial \bar{X}_k} + J^{-1} \bar{b}_i\,, \tag{14}$$

$$J \overline{K}^{-1} \frac{\partial \bar{p}}{\partial \bar{t}} + G_{jk} \frac{\partial \bar{v}_k}{\partial \bar{X}_j} = 0, \tag{15}$$

where $\overline{K} = K/p^*$, $\bar{b}_1 = 0$, and $\bar{b}_2 = -1$. Note that the deformation gradient components G_{ij}, and hence the Jacobian J, are left unaltered since the same length unit, H^*, is used to normalize the horizontal as well as the vertical coordinates; otherwise, they should be re-scaled appropriately as well.

3. Finite Element Method Description

The water flow governing equations for the unknown velocity and pressure fields, in their dimensionless forms expressed by Eq. (14) and (15), have been solved numerically by a finite element method. The solution has been based on a weak formulation

of the problem equations, by applying the Galerkin method (Zienkiewicz and Taylor 2000b). The water flow domain is discretized by imposing a mesh consisting of triangular elements, see Fig. 2. The mesh, for the referential configuration at time $t = 0$, is generated in such a way that first a structured mesh of triangles with their vertices uniformly distributed along the X_1 and X_2 axes is created for a rectangular domain, and then, to account for the bed geometry and the initial free surface elevation at a given X_1, the vertices are moved along the X_2 axis so that they remain uniformly distributed along the verticals.

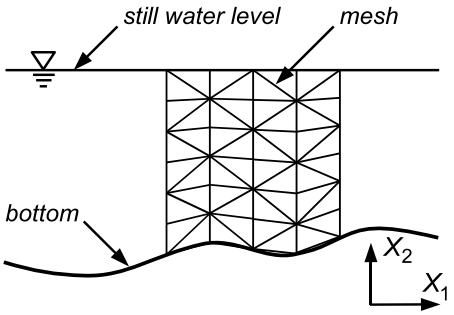

Fig. 2. Finite element mesh in the initial fluid configuration

The triangular elements with four nodes are used. Three nodes are located at the triangle vertices, and the fourth node is at the triangle barycentre. At the vertex nodes the discrete values of the unknown velocity components are defined, while at the middle node the pressure is defined. Thus, at each element there are seven discrete values to be calculated, six velocity components and one pressure value. The above implies that the linear approximation of the velocity field $\bar{\boldsymbol{v}}(\overline{\boldsymbol{X}}, \bar{t})$ within an element is assumed, while the pressure field $\bar{p}(\overline{\boldsymbol{X}}, \bar{t})$ is supposed to be constant therein. More details on the discretization method, and the formulae for calculating the element matrices, can be found in the previous work of the author (Staroszczyk 2007). Aggregation of the global matrices and vectors from the respective individual element matrices and vectors in a manner typical of the finite element method leads to a set of equations that can be expressed, in matrix notation, in the form

$$\boldsymbol{C}\dot{\boldsymbol{u}}(t) + \boldsymbol{K}\boldsymbol{u}(t) = \boldsymbol{f}(t), \quad \boldsymbol{u}(0) = \boldsymbol{u}_0\,. \tag{16}$$

In the above relation, $\boldsymbol{u}$ is the vector of unknown discrete values of velocities and pressures in all nodal points of the discrete system, $\boldsymbol{f}$ is the loading vector, and $\boldsymbol{u}_0$ represents the initial solution vector (nodal values of the velocity and pressure fields at time $t = 0$).

Matrix equation (16) forms a system of first-order differential equations in which the matrices $\boldsymbol{C}$ and $\boldsymbol{K}$ and the vector $\boldsymbol{f}$ all depend on the components of the deformation gradient tensor $\boldsymbol{G}$. Hence, $\boldsymbol{C}$, $\boldsymbol{K}$ and $\boldsymbol{f}$ are all functions of the solution

vector $\boldsymbol{u}$. In order to integrate this non-linear system of equations, a single-step scheme, known as the weighted average θ-method, has been used. Application of this method to Eq. (16) yields the following system of algebraic equations:

$$(\boldsymbol{C} + \Delta t\,\theta \boldsymbol{K})\,\boldsymbol{u}_{n+1} = [\boldsymbol{C} - \Delta t\,(1-\theta)\boldsymbol{K}]\,\boldsymbol{u}_n + \Delta t \bar{\boldsymbol{f}}_n \quad (n = 0, 1, 2, \ldots), \tag{17}$$

which connects the solution vectors $\boldsymbol{u}_n$ and $\boldsymbol{u}_{n+1}$ at two consecutive time levels, t_n and $t_{n+1} = t_n + \Delta t$, with Δt denoting the time step length. The vector $\bar{\boldsymbol{f}}_n$ is the time-averaged loading vector which, assuming its linear variation between $t = t_n$ and $t = t_{n+1}$, is expressed by

$$\bar{\boldsymbol{f}}_n = (1-\theta)\boldsymbol{f}_n + \theta \boldsymbol{f}_{n+1}\,. \tag{18}$$

In the calculations, the value of the weighting parameter θ was adopted to be close to unity, which means that nearly the fully implicit backward scheme was employed, ensuring thus good numerical stability of the algorithm, at the cost, however, of some loss of computational accuracy (the best accuracy would be achieved for $\theta = 0.5$, but in this case the scheme is less stable than for $\theta \sim 1$).

Since the matrices $\boldsymbol{C}(\boldsymbol{u})$ and $\boldsymbol{K}(\boldsymbol{u})$ appearing in Eq. (17) change as we progress from the old time level t_n to the new level t_{n+1}, the solution vector u_{n+1} does not satisfy, in general, the equation (17). For this reason, correction of the solution is required in order to reach equilibrium before to proceed to the next time step. From among a few possible approaches, the direct (Picard) iteration method has been applied, in which the current approximation to the solution vector $\boldsymbol{u}^i_{n+1}$ ($i = 0, 1, 2, \ldots$) is immediately used to modify the matrices $\boldsymbol{C}$ and $\boldsymbol{K}$ and the forcing vector $\bar{\boldsymbol{f}}$ in Eq. (17), before moving on to the next iteration $i + 1$. Usually, depending on the time interval length Δt, four to six iterations were needed to compute the solution vector $\boldsymbol{u}_{n+1}$ with the relative error (of the solution vector norms) between two successive iterations not exceeding 10^{-8}.

The solution of the system of algebraic equations (17) requires a special treatment, since the matrix $(\boldsymbol{C} + \Delta t\,\theta \boldsymbol{K})$ on the left-hand side of Eq. (17) is ill-conditioned, reflecting the fact that we deal with the problem of nearly-incompressible fluid flow. For this reason, the calculation of an accurate solution of Eq. (17) encounters certain difficulties, and an application of some stabilization method is usually necessary to avoid numerical oscillations to appear in the results obtained. From among a number of available methods, an approach known as the augmented Lagrangian technique (Zienkiewicz and Taylor 2000b) is employed here. To outline this method, let us express the system of equations (17) in the following form:

$$\begin{bmatrix} \boldsymbol{A} & \boldsymbol{B} \\ \boldsymbol{B}^T & \boldsymbol{E} \end{bmatrix} \begin{Bmatrix} \bar{\boldsymbol{v}}_{n+1} \\ \bar{\boldsymbol{p}}_{n+1} \end{Bmatrix} = \begin{Bmatrix} \bar{\boldsymbol{q}}^{(1)}_n \\ \bar{\boldsymbol{q}}^{(2)}_n \end{Bmatrix}, \tag{19}$$

where $\boldsymbol{A}$ and $\boldsymbol{E}$ are square matrices, and the solution vector $\boldsymbol{u}$ is split into two parts: $\bar{\boldsymbol{v}}$ containing all discrete velocities, and $\bar{\boldsymbol{p}}$ containing all discrete pressures. Similarly, the right-hand side vector is split into two parts, $\bar{\boldsymbol{q}}^{(1)}$ and $\bar{\boldsymbol{q}}^{(2)}$, as well.

In the scaled variables, in which the flow equations are solved, the typical non-zero entries in $\boldsymbol{A}$ turn out to be by several orders of magnitude larger than the non-zero entries in $\boldsymbol{E}$ (in the case of a fully incompressible fluid, for which $K \to \infty$, the latter matrix would be singular). Such considerable differences between the magnitudes of elements of $\boldsymbol{A}$ and $\boldsymbol{E}$, including the diagonal elements, are an undesirable feature which leads to large numerical errors to accumulate during the solution process. Therefore, to reduce this near-singular behaviour of the system, the matrix $\boldsymbol{E}$ is augmented, by subtracting the term $\alpha\bar{\boldsymbol{p}}$ from each side of the second matrix equation in Eq. (19), and then solving the resulting equations by iterations. Hence, the modified system of equations is expressed in the form

$$\begin{bmatrix} \boldsymbol{A} & \boldsymbol{B} \\ \boldsymbol{B}^T & \hat{\boldsymbol{E}} \end{bmatrix} \begin{Bmatrix} \bar{\boldsymbol{v}}_{n+1}^{(k+1)} \\ \bar{\boldsymbol{p}}_{n+1}^{(k+1)} \end{Bmatrix} = \begin{Bmatrix} \bar{\boldsymbol{q}}_n^{(1)} \\ \bar{\boldsymbol{q}}_n^{(2)} - \alpha\bar{\boldsymbol{p}}_{n+1}^{(k)} \end{Bmatrix} \quad (k = 0, 1, \ldots), \tag{20}$$

where the augmented matrix $\hat{\boldsymbol{E}}$ is given by

$$\hat{\boldsymbol{E}} = \boldsymbol{E} - \alpha\boldsymbol{I}. \tag{21}$$

Now, the above iterative system is solved, at a given time level t_n, by starting the calculations from $\bar{\boldsymbol{p}}_{n+1}^{(0)} = \bar{\boldsymbol{p}}_n$. The value of the parameter α which controls the stabilization process should be selected in such a way that the number of iterations in Eq. (20) is minimized.

4. Examples of the Model Application

The finite element method, outlined in the preceding section, has been employed to simulate the gravity wave propagation in water of non-uniform depth. The following parameters have been adopted to describe the water properties: the density $\varrho_0 = 10^3$ kg m^{-3}, the viscosity $\mu = 1.01 \times 10^{-3}$ Ns m^{-2}, and the compressibility modulus $K = 2.04 \times 10^9$ Pa.

The flow problem under investigation has been solved in domains of simple bottom geometry, sketched in Fig. 3. Three cases of the bottom geometry have been considered to represent idealized beach profiles: a uniformly inclined beach, with a slope $1/m$, ending at a vertical wall, (a); a uniformly inclined beach followed by a constant-depth region, (b); and a more complex profile with two inclined parts, both with the same slope $1/m$, separated by a flat horizontal section, (c). In all the cases, a surface wave is supposed to be generated by a movement of a rigid vertical wall situated at the left-hand end of the flow domain (that is, at $X = 0$). The region adjacent to the moving wall, of a length L_1, has a constant depth H. The dimensions of the flow domain have been assumed as those of a laboratory flume. Hence, the still water depth is set to $H = 60$ cm, and the total length of the water domain, in cases (a) and (b), is $L = 15$ m; in case (3), depending on the slope $1/m$, the length L can be smaller.

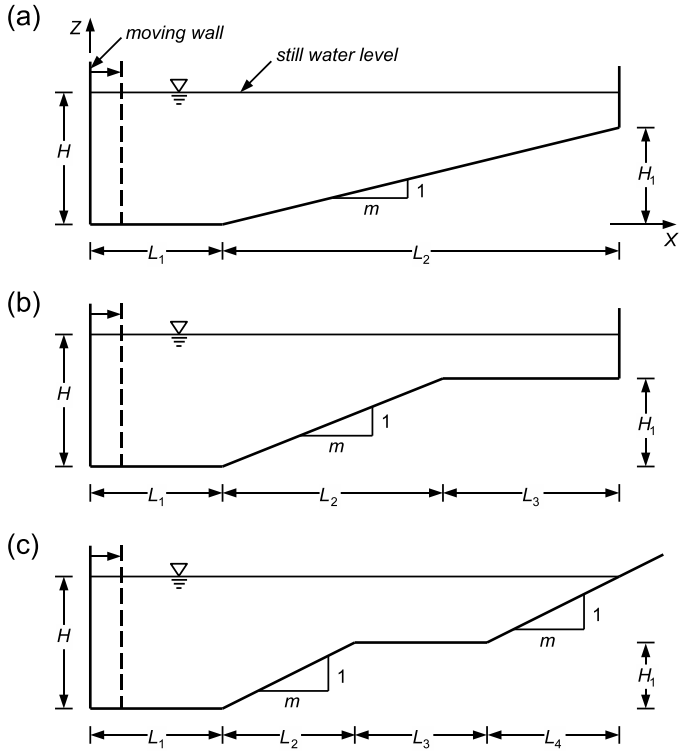

Fig. 3. Three different bed profiles

In the calculations, the length scale H^*, used to normalize the flow field variables, has been chosen to be equal to the depth H, that is, $H^* = 60$ cm. The latter value determines, see Eq. (13), the other scaling parameters: $v^* = 2.43$ m s^{-1} for velocities, $p^* = 5.88 \times 10^3$ Pa for pressures, and $\mu^* = 1.46 \times 19^3$ Ns m^{-2} for the viscosity.

The results presented below have been obtained by imposing on the fluid domain a grid of triangular finite elements consisting of 10 'layers' of elements along the vertical axis, and 250 'columns' of elements along the horizontal axis. Thus, the mesh included 5000 elements (each of the initial horizontal side equal to 6 cm, the latter being also the maximum vertical side of the triangles), with the total number of 10 522 degrees of freedom. The time integration was conducted by using a constant-length time increment $\Delta t = 10^{-3}$ s.

It has been assumed that the fluid is at rest at times $t < 0$, and is set in motion by the vertical wall which, starting at $t = 0$, makes a single translational movement in the horizontal direction by a distance D_0, and then stops. The following smooth function, with continuous first and second-order time derivatives at $t = 0$, has been adopted for illustrations to describe the horizontal displacement $d_0(t)$ of the generator:

$$d_0(t) = D_0\left[1 - \exp\left(-\tau^3\right)\right], \quad \tau = \frac{t}{T_0}, \tag{22}$$

where T_0 is a characteristic time of the wave-maker movement.

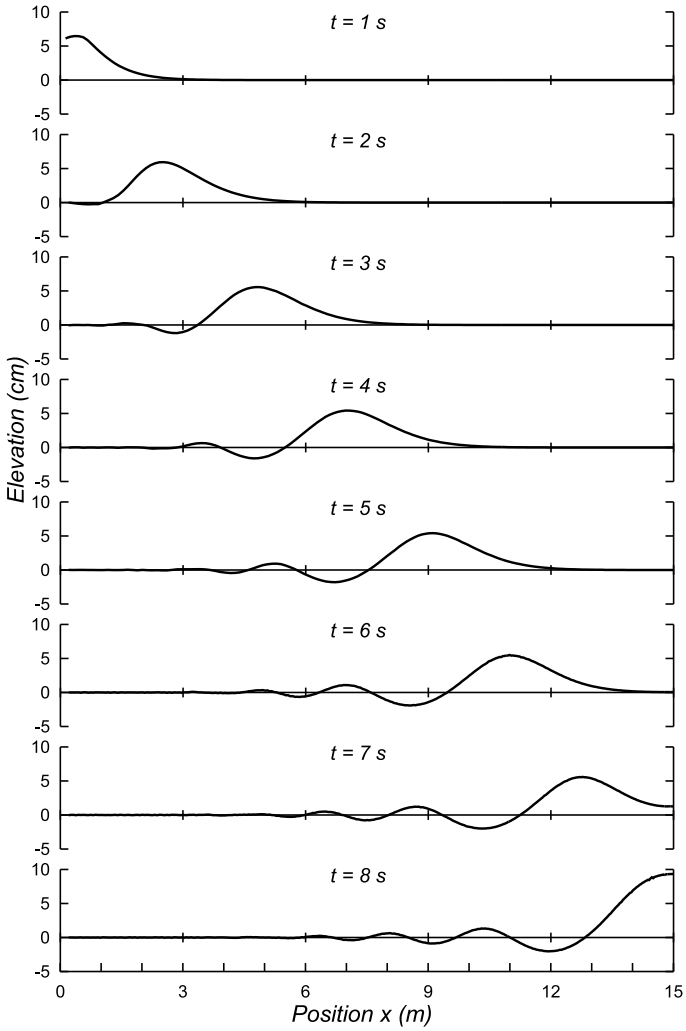

Fig. 4. Transformation of the wave propagating along the flume with the bottom profile shown in Fig. 3a, for the total wave-maker horizontal displacement $D_0 = 20$ cm and the characteristic time $T_0 = 1.0$ s

Figures 4 and 5 illustrate the transformation of a gravity wave propagating over the bottom shown in Fig. 3a, with the dimensions $L_1 = 3$ m, $L_2 = 12$ m and $H_1 = 40$ cm. Hence, the slope of the uniformly inclined part of the bottom is 1/30, and the minimum still water depth is equal to 20 cm at $X = 15$ m. The wave

motion is induced by moving the maker wall by a distance of $D_0 = 20$ cm, with the characteristic time $T_0 = 1$ s. Such a wall movement produces, in the case of the horizontal bed, a transient wave which has a maximum elevation of about 6.5 cm.

The plots in Figure 4 show the behaviour of a wave as it travels the whole length of the flume and then reflects at the rigid wall at $X = 15$ m, giving rise to the interaction between the waves propagating in opposite directions. It can be noted that, due to the very mild bottom slope, equal here to 1/30, the overall behaviour of the wave is rather little affected by the change of the water depth. This is confirmed by the plots in Figure 5, comparing the profiles of the waves, both induced by the same wall movement at $X = 0$, propagating over the horizontal bottom and that sketched in Fig. 3a. The plots in Fig. 5a display a small, but steady, decrease in the height of the wave front with an increasing distance travelled by the wave. Compared to that, the wave propagating over the shoaling bottom, see Fig. 5b, retains approximately the same height, which means that (in this particular situation considered) the shoaling and dispersive effects are roughly counter-balanced. Evidently, a more significant is the effect of the sloping bed on the wave length, as the shortening and steepening of the wave profile are clearly noticed in Fig. 5b.

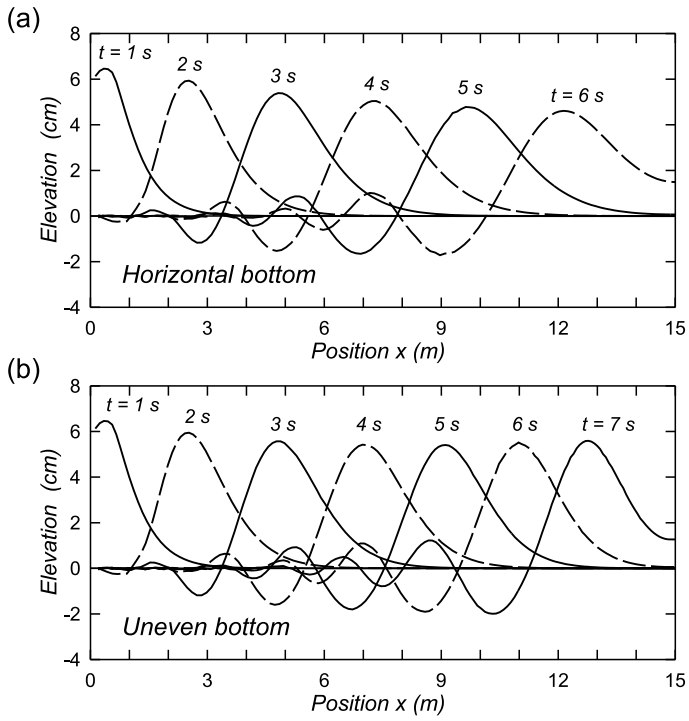

Fig. 5. Evolution of the free-surface elevation for the wave propagating: (a) over the horizontal bed, (b) over the bed defined in Fig. 3a ($D_0 = 20$ cm, $T_0 = 1.0$ s)

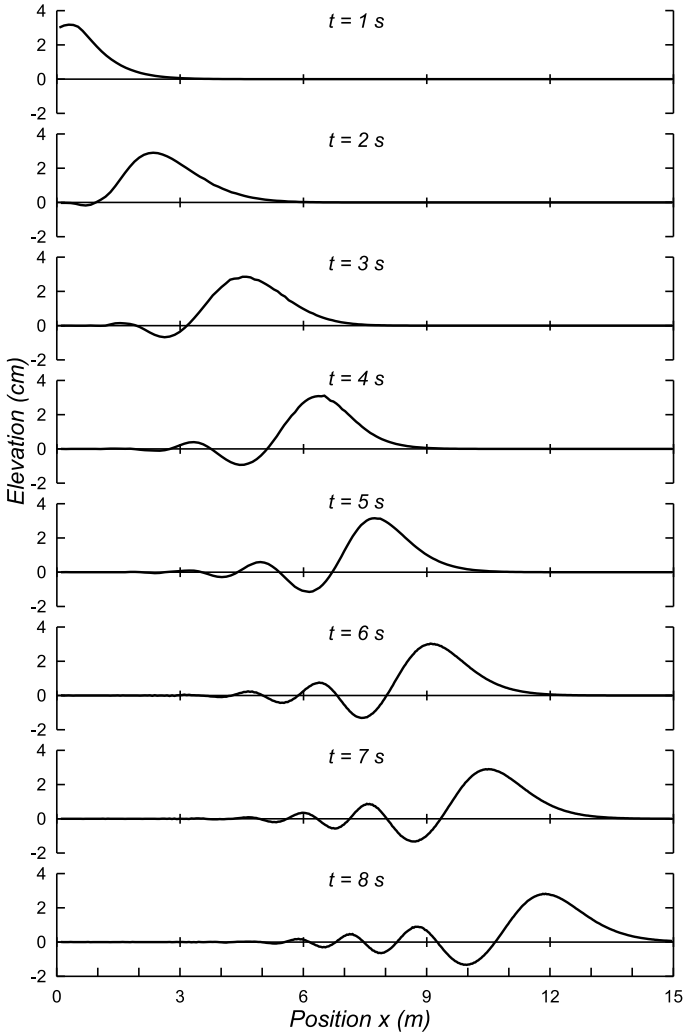

Fig. 6. Transformation of the wave propagating along the flume with the bottom profile shown in Fig. 3b, for the slope of the inclined section equal to 1/10, for the total wave-maker horizontal displacement $D_0 = 10$ cm and the characteristic time $T_0 = 1.0$ s

Figures 6 and 7 illustrate the transformation of a wave propagating over the bed defined in Fig. 3b. The initial horizontal section of the bed has again a length of $L_1 = 3$ m, and the other horizontal section is raised by $H_1 = 40$ cm above the latter. Three different slopes of the shoaling part of the bed have been assumed, namely: 1/15, 1/10 and 1/5, in order to investigate their influence on the wave propagation. The plots show the behaviour of the wave which is excited by the wall moving with the amplitude $D_0 = 10$ cm, with the characteristic time $T_0 = 1$ s.

Figure 6 shows the evolution of the water surface elevation for the case of the inclined bottom with the slope of 1/10, extending between the points $X = 3$ and

$X = 7$ m. It can be seen that, referring to the wave depicted in Fig. 4, also in this case of the bottom geometry no significant changes in the wave front height occur, even though the water depth has decreased three-fold. Yet again, the bed topography has a more pronounced effect on the wave shape, reflected by shortening and steepening of the wave profile once it has passed the sloping section of the bottom. One can notice some oscillations of a numerical character which appear in the plots for $t = 3$ and $t = 4$ s, that is, when the front of the wave is currently propagating over the inclined bed. These numerical oscillations are subsequently smoothed out, as can be observed in the plots for the later times.

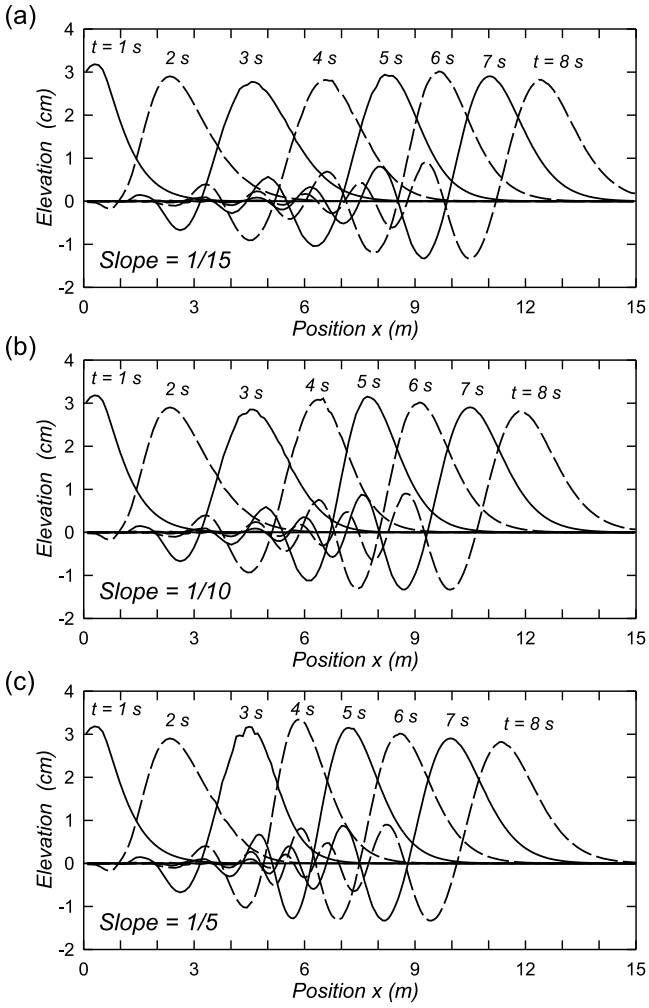

Fig. 7. Evolution of the free-surface elevation for the wave propagating over the bottom profile defined in Fig. 3b, for three different slopes (1/15, 1/10 and 1/5) of the inclined section of the bed ($D_0 = 10$ cm, $T_0 = 1.0$ s)

Figure 7 demonstrates the influence of the slope of the shoaling part of the bottom on the wave shape. Hence, the wave profiles, still for the bed geometry defined in Fig. 3b, are compared for the bed slopes equal to 1/15, 1/10 and 1/5, respectively. One can observe some increase in the leading wave crest height as the wave is propagating through the shoaling zone. The most noticeable increase occurs in the case of the largest slope, when the wave becomes higher by about 20% compared to its height at the beginning of the sloping section.

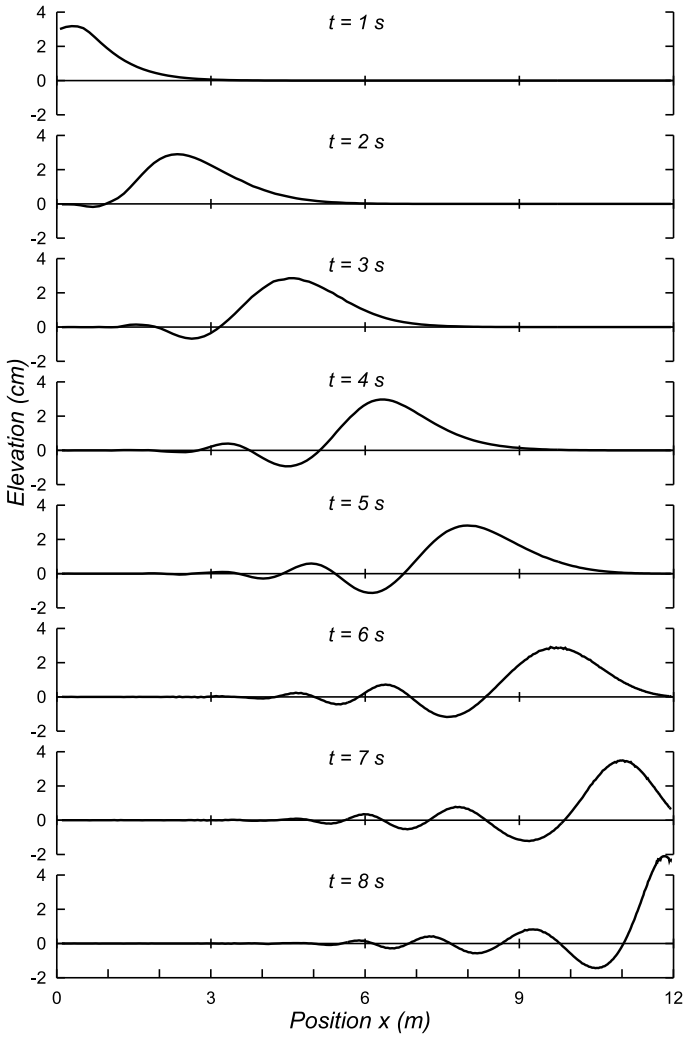

Fig. 8. Transformation of the wave propagating along the flume with the bottom profile shown in Fig. 3c, for the slopes of the inclined sections equal to 1/10, for the total wave-maker horizontal displacement D_0 = 10 cm and the characteristic time T_0 = 1.0 s

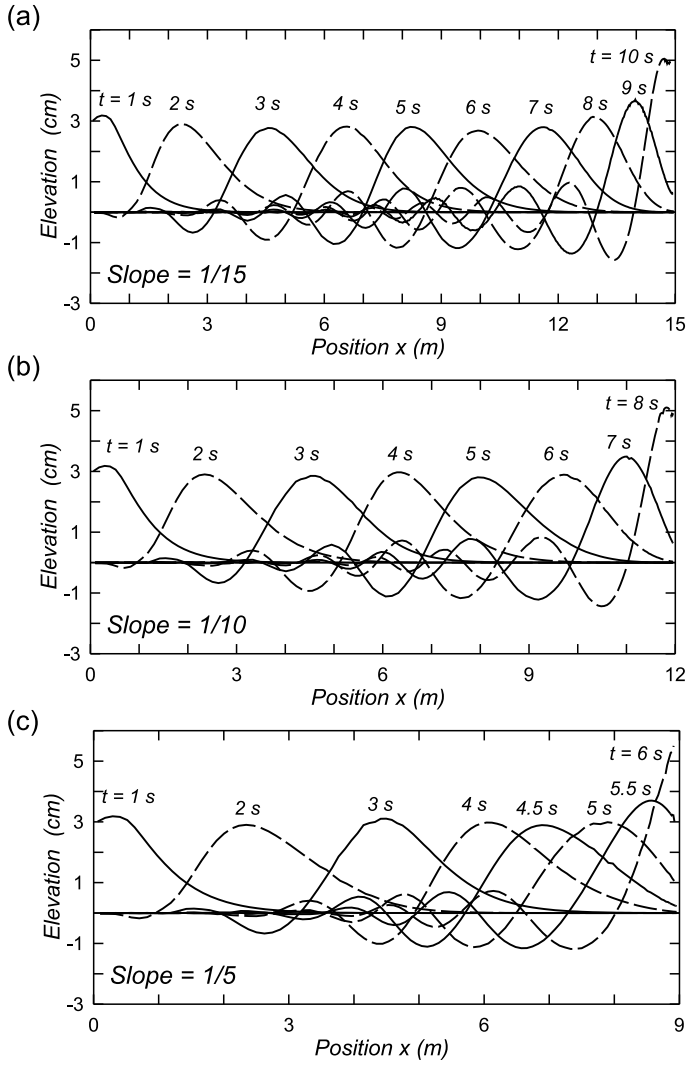

Fig. 9. Evolution of the free-surface elevation for the wave propagating over the bottom profile defined in Fig. 3c, for three different slopes (1/15, 1/10 and 1/5) of the inclined section of the bed (D_0 = 10 cm, T_0 = 1.0 s)

Figures 8 and 9 illustrate the evolution of a transient wave propagating over the bed defined in Fig. 3c, with two sloping sections of the bottom. Yet again, the initial horizontal section of the bed has a length of L_1 = 3 m, and the other horizontal section, at the height of H_1 = 30 cm above the latter, has the same length, that is, L_3 = 3 m as well. Both shoaling sections are assumed to have the same slopes. The plots show the behaviour of the initially the same wave as that in Figs. 6 and 7, that is, generated with the wave-maker parameters D_0 = 10 cm and T_0 = 1 s.

The plots in Figure 8 show the transformation of the wave when the inclined bottom sections have the slopes equal to 1/10 (hence, $L_2 = L_4 = 3$ m). In this particular bed geometry, the initial total length of the flow domain is 12 m. It is clearly seen that more significant changes in the wave profile take place over the second shoaling section of the bed (for $X > 9$ m), that is in the region of much shallower water. The discrete model predicts over a two-fold increase in the wave height near the end of the flow domain, before the simulations break down due to numerical instabilities which prevent the scheme from calculating a convergent solution.

Finally, Figure 9 illustrates the transformation of the wave profiles for different slopes of the inclined sections of the bottom for the geometry defined in Fig. 3c. Hence, the results for the slopes of 1/15, 1/10 and 1/5 are compared. Note the distinct horizontal scales in the three plots.

5. Conclusions

A finite element model has been constructed to analyse the plane problem of gravity waves propagating in water of non-uniform depth. A Lagrangian form of the FE method has been applied, with a convecting grid of discrete points moving with the material particles of the fluid. The model has been used to simulate the behaviour of a transient-type wave travelling over the bottom of a simple shape, with the focus on the transformation of the wave profile in response to varying bed conditions. Hence, three cases of bottom configurations, idealizing typical beach profiles, have been investigated, and the results of numerical simulations, showing the evolution of the free-surface elevation, have been illustrated.

The numerical analysis has shown that the proposed method is capable of successful dealing with non-linear problems involving water waves propagating over uneven beds with gentle and moderate slopes. In its present formal description, the model accounts for the phenomena of fluid compressibility and viscosity, introduced with the hope to enhance the numerical stability of the model. However, the results of numerical tests, in which the magnitudes of parameters describing the water compressibility and viscosity were varied to examine their effect on the stability of calculations, have shown that the presence of extra terms in the equations (compared with the standard approach of an incompressible and inviscid fluid) does not improve significantly the computational performance of the model. It seems that before the model can be applied to solving more challenging problems of non-linear waves propagation over steep beds of an arbitrary geometry, some extensions are necessary in order to improve its numerical robustness. In first place, it would be desirable to implement one of the special techniques that have been developed in recent years for stabilizing the numerical schemes for solving incompressible, or nearly incompressible, fluid flows, but without introducing any unphysical quantities into the description (such as introduction of diffusive terms in the equations,

introduction of artificial viscosity terms, the penalty method, etc.). Also, it seems that the use of higher-order finite elements, enabling a better spatial approximation of the variables involved, can help to enhance the model performance.

References

Aubry R., Idelsohn S. R. and Oñate E. (2005) Particle finite element method in fluid-mechanics including thermal convection-diffusion, *Comput. Struct.*, **83** (17–18), 1459–1475.

Braess H. and Wriggers P. (2000) Arbitrary Lagrangian Eulerian finite element analysis of free surface flows, *Comput. Meth. Appl. Mech. Eng.*, **190** (1–2), 95–109.

Chadwick P. (1999) *Continuum Mechanics: Concise Theory and Problems*, Dover, Mineola, New York, 2nd edn.

Dingemans M. W. (1997) *Water Wave Propagation over Uneven Bottoms*, World Scientific, Singapore.

Idelsohn S. R., Oñate E. and Del Pin F. (2004) The particle finite element method: a powerful tool to solve incompressible flows with free-surfaces and breaking waves, *Int. J. Numer. Meth. Eng.,* **61** (7), 964–989.

Idelsohn S. R., Oñate E., Del Pin F. and Calvo N. (2006) Fluid-structure interaction using the particle finite element method, *Comput. Meth. Appl. Mech. Eng.,* **195** (17–18), 2100–2123.

Löhner R., Sacco C., Oñate E. and Idelsohn S. (2002) A finite point method for compressible flow, *Int. J. Numer. Meth. Eng.,* **53** (8), 1765–1779.

Oñate E., Idelsohn S. R., Zienkiewicz O. C., Taylor R. L. and Sacco C. (1996) A stabilized finite point method for analysis of fluid mechanics problems, *Comput. Meth. Appl. Mech. Eng.,* **139** (1–4), 315–346.

Ortega E., Oñate E. and Idelsohn S. (2007) An improved finite point method for tridimensional potential flows, *Comput. Mech.,* **40** (6), 949–963.

Parrinello F. and Borino G. (2007) Lagrangian finite element modelling of dam–fluid interaction: Accurate absorbing boundary conditions, *Comput. Struct.,* **85** (11–14), 932–943.

Rabier S. and Medale M. (2003) Computation of free surface flows with a projection FEM in a moving mesh framework, *Comput. Meth. Appl. Mech. Eng.,* **192** (41–42), 4703–4721.

Radovitzky R. and Ortiz M. (1998) Lagrangian finite element analysis of Newtonian viscous flow, *Int. J. Numer. Meth. Eng.,* **43** (4), 607–619.

Ramaswamy B. and Kawahara M. (1987) Lagrangian finite element analysis applied to viscous free surface flow, *Int. J. Numer. Meth. Fluids,* **7** (9), 953–984.

Souli M. and Zolesio J. P. (2001) Arbitrary Lagrangian-Eulerian and free surface methods in fluid mechanics, *Comput. Meth. Appl. Mech. Eng.,* **191** (3–5), 451–466.

Staroszczyk R. (2007) A Lagrangian finite element treatment of transient gravitational waves in compressible viscous fluids, *Arch. Hydro-Eng. Environ. Mech.,* **54** (4), 261–284.

Stoker J. J. (1957) *Water Waves. The Mathematical Theory with Applications*, Inter-Science, New York.

Wehausen J. V. and Laitone E. V. (1960) Surface waves, In: *Encyclopedia of Physics* (ed. S. Flügge), Vol. IX, Springer, Berlin.

Zienkiewicz O. C. and Taylor R. L. (2000a) *The Finite Element Method. Fluid Dynamics*, Vol. 3. Butterworth-Heinemann, Oxford, 5th edn.

Zienkiewicz O. C. and Taylor R. L. (2000b) *The Finite Element Method. The Basis*, Vol. 1. Butterworth-Heinemann, Oxford, 5th edn.